JOURNAL OF PROPULSION AND POWER
Vol. 12, No. 1, January–February 1996

Large-Displacement Structural Durability Analyses of Simple Specimens Emulating Rocket Chambers

Vinod K. Arya*
University of Akron, Akron, Ohio 44325
and
Gary R. Halford† and Leonard J. Westfall‡
NASA Lewis Research Center, Cleveland, Ohio 44135

Large-displacement elastic and elastic–plastic, stress–strain finite element analyses (FEA) of an oxygen-free high-conductivity (OFHC) copper plate specimen were performed using an updated Lagrangian formulation. The plate specimen is intended for low-cost experiments that emulate the most important thermomechanical loading and deformation/failure modes of a more complex rocket thrust chamber. The plate, which is loaded in bending at 593°C, contains a centrally located and internally pressurized channel. The cyclic crack initiation lives were estimated using the results from the FEA analyses and isothermal strain-controlled low-cycle fatigue data for OFHC copper at 538°C. A comparison of the predicted and experimental cyclic lives showed that an elastic analysis predicts a longer cyclic life than that observed in experiments by a factor greater than 4. The results from elastic–plastic analysis for the plate bend specimen, however, predicted a cyclic life in close agreement with experiment, thus justifying the need for the more rigorous stress–strain analysis.

Nomenclature

ε = strain

Subscripts
e = effective
1, 2, 3 = components of principal strain

Introduction

ONE of the important life-limiting failure modes encountered by the rocket thrust chamber liner of the Space Shuttle main engine is thermal/mechanical ratcheting of the thin (0.06-cm) wall of copper alloy (NARloy Z) between the fuel/coolant channels and the hot gas wall. The racheting of material is toward the hot gas path side of the liner. A similar deformation/failure mode is observed in subscale thrust chambers made of oxygen-free, high-conductivity (OFHC) copper.[1,2] When viewed in transverse (to the gas flow) cross section, the initially rectangular fuel/coolant channels tend to develop a doghouse shape with the roof pointed toward the centerline of the thrust chamber (see cross-sectional view of subscale rocket thrust chamber in Fig. 1, taken from Ref. 3). This deformation mode feeds on itself and causes the thin wall to become ever thinner. The thinned area may rupture eventually and dump valuable hydrogen fuel into the nozzle where it is burned without a significant propulsive effect. The rate of thinning (i.e., ratcheting) has been shown analytically by Arya and Arnold[4] to be temperature, pressure, and cycle dependent. New geometric designs or new materials are required to either eliminate or mitigate this deformation mode that leads to eventual cracking of the thinned channel wall. Surely, if the cyclic rate of ratcheting could be reduced, the cyclic life at rupture could be extended.

Received July 22, 1994; revision received April 19, 1995; accepted for publication April 19, 1995. This paper is declared a work of the U.S. Government and is not subject to copyright protection in the United States.

*Visiting Associate Professor, Department of Mathematical Sciences.
†Senior Scientific Technologist, Structures Division.
‡Research Engineer, Retired, Materials Division.

Full-scale thrust chambers are too prohibitively expensive to build and test for the purpose of investigating new configurations and construction materials. Thus, subscale liners that retain the important features of a full-scale liner have been designed, built, analyzed, and tested.[1,2] These are also expensive to build and test. Furthermore, the turnaround time from idea (new material, new channel configuration, fabrication, technique, etc.) to experimental verification is unacceptably long (typically about 2 years). Thus, tremendous savings in time and expense can be achieved if a simpler, less expensive benchmark configuration can successfully emulate the basic structural loading, deformation response, and failure mode of full-size hardware.

A relatively simple plate bend specimen has been found to capture the essence of the loadings and deformation/failure response modes found in high-heat-flux, high-thermal-con-

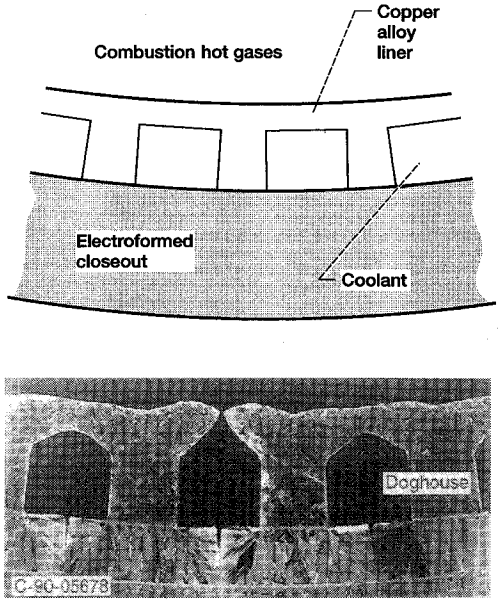

Fig. 1 Coolant channels of subscale rocket chamber a) before and b) after repeated firings.[3]

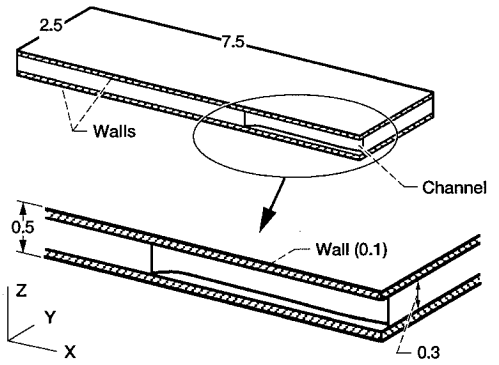

Fig. 2 Plate bend specimen (one-quarter). (All dimensions are in centimeters.)

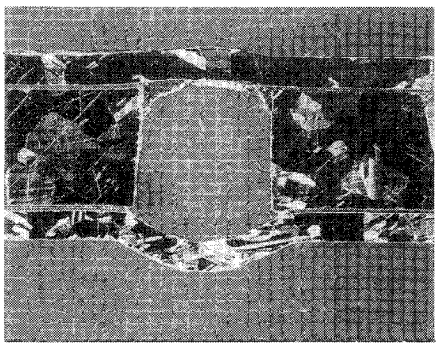

Fig. 3 Deformed channel of plate specimen showing doghouse effect.

ductivity rocket thrust chamber liners. The bend specimen is a flat plate with an internally pressurized single longitudinal channel that is located along the center of the plate (Fig. 2). The Appendix gives the manufacturing details of this specimen.

Large-displacement tests of the plate specimen were performed isothermally in air at 593°C in four-point loading to simulate the large cyclic thermal strains experienced by the full-scale rocket thrust chamber liner. Bending strain gradients in the plate also simulate thermal strain gradients in the nozzle liner. This specimen exhibits a bulging deformation mode and a location of cracking (Fig. 3) that have been observed in thrust chamber liners. Therefore, this specimen approximates the requirements of a less expensive benchmark configuration that can be used to analytically assess and experimentally verify new materials and design concepts for longer lived rocket chambers.

This article analytically investigates the loading, deformation, and life of the surrogate bend specimen. Because the ratio of the maximum deflection of the plate to its thickness is large (greater than 0.75), small-displacement analyses for the problem produce inaccurate results. Large-displacement analyses are therefore required. Although the test temperature is within the creep range, the testing frequency of 0.11 Hz is high enough to justify neglecting time-dependent (creep) effects. The investigations reported herein were conducted by performing large-displacement finite element analyses (FEA) in conjunction with elastic and elastic–plastic constitutive models. The analytical results are displayed and discussed.

FEA

Finite Element Model

The geometry and dimensions of the specimen and channel are given in Fig. 2. Solid eight-noded brick elements with an assumed strain formulation were utilized to model the pressurized (6.2-MPa) center channel of the specimen. Because of the geometric and loading symmetry, only one-quarter of the specimen was modeled. A sensitivity study of the effect of mesh density on the results showed that a large number of elements was required for accurately capturing the high-bending strain gradients. The presence of internal pressure in the channel, in addition to the bending gradients, necessitated the use of an even finer mesh in the channel region of the specimen. This finite element model is shown in Fig. 4 and consists of 3330 elements and 4463 nodes.

Approximate Shape of Bent Specimen (Plate)

Only the maximum deflection occurring at the center of the plate was experimentally measured; hence, to determine the deflections at all other points of the plate (and its bent shape at maximum deflection), an approximate elastic analysis was performed by modeling the whole plate as a solid thick plate excluding the channel under uniform load transverse to the plate. The load was analytically increased until the calculated deflection at the center was equal to the value measured in experiments. The deflections at all other points (nodes) of the plate were also recorded at this time. These displacements were later used to perform the elastic and elastic–plastic FEA by treating these latter analyses as displacement-controlled boundary value problems. All FEA were performed by using the finite element program MARC.[5] The undeformed and (calculated) deformed shapes of the solid thick plates subject to these FEA are shown in Fig. 5. The displacements shown are exaggerated by a factor of 5. Only a half-cycle of load has been analyzed.

Elastic Analysis

A one-fourth segment of the pressurized and deformed (bent) single-channel plate is shown in Fig. 6. The undeformed configuration is presented for comparison. Deformation displacements are exaggerated by a factor of 5 to clearly distinguish the two configurations. An elastic stress–strain structural analysis was performed using a finite element discretization of this segment as described in the section FEA. Because the

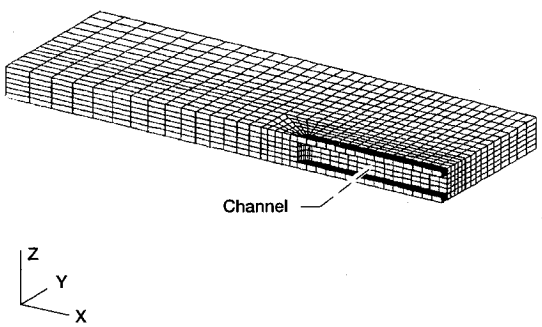

Fig. 4* Finite element model of plate bend specimen (3330 elements; 4463 nodes).

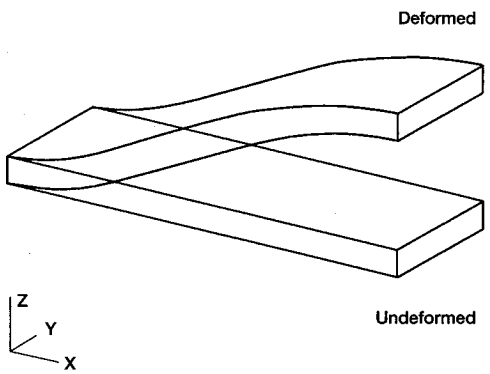

Fig. 5 Undeformed and deformed shapes of thick plate. (Deformations are magnified by a factor of 5.)

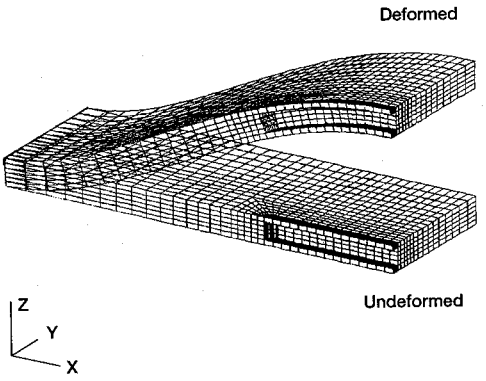

Fig. 6 Deformed and undeformed shapes of segment. (Deformations are magnified by a factor of 5.)

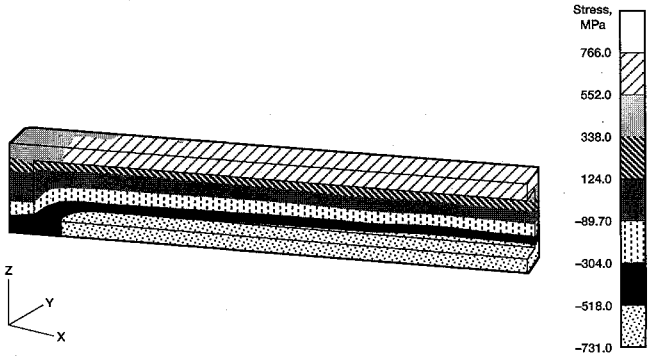

Fig. 7 *X* stress in channel wall; elastic analysis.

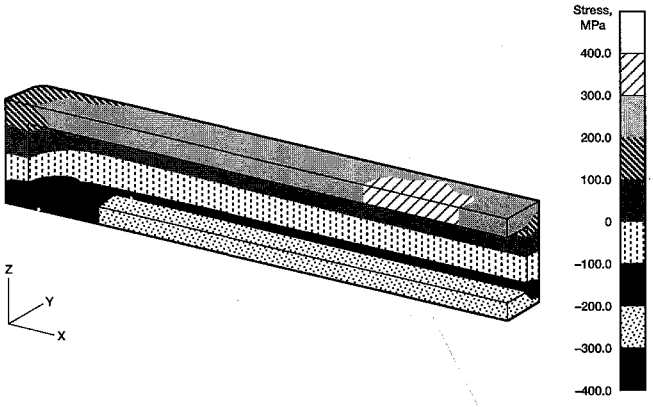

Fig. 8 *Y* stress in channel wall; elastic analysis.

problem involves large displacements of the segment in the *XZ* plane, a large-displacement analysis using an updated Lagrangian formulation was adopted. The channel region of the specimen is of greatest interest; thus, only those figures that exhibit the stress and strain distributions in this region are included.

The longitudinal (*X*-direction) stress in the vicinity of the channel is shown in Fig. 7. A typical bending stress distribution is observed with tension on the upper surface, compression on the lower surface, and a neutral axis of zero stress in the middle. The maximum elastically calculated longitudinal stress in the channel is about 766 MPa. The stresses in the *Y* and *Z* directions are shown in Figs. 8 and 9, respectively. The *Y* and *Z* stresses have maximum magnitudes of about 350 and 260 MPa, respectively. These stress values far exceed the 30 MPa 0.2% offset yield strength of OFHC copper at 593°C.

The strain distribution in the channel in the *X*, *Y*, and *Z* directions is shown in Figs. 10–12, respectively. The maxi-

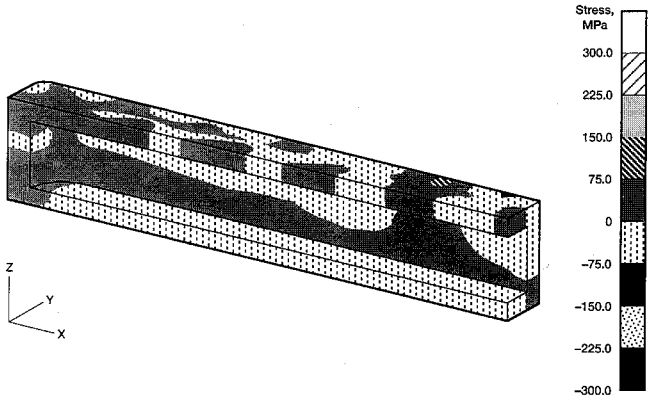

Fig. 9 *Z* stress in channel wall; elastic analysis.

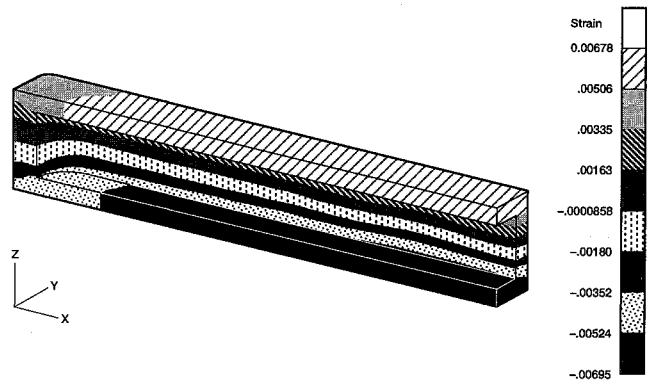

Fig. 10 *X* strain in channel wall; elastic analysis.

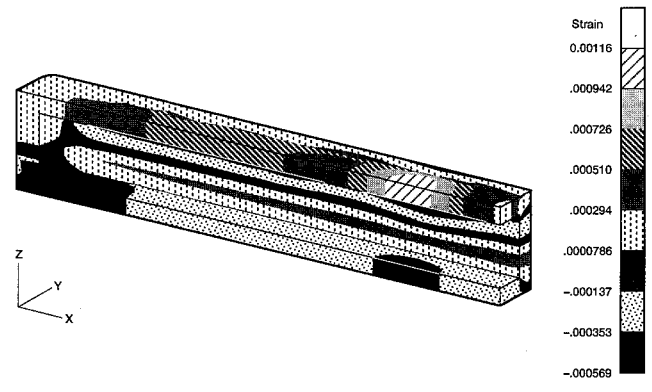

Fig. 11 *Y* strain in channel wall; elastic analysis.

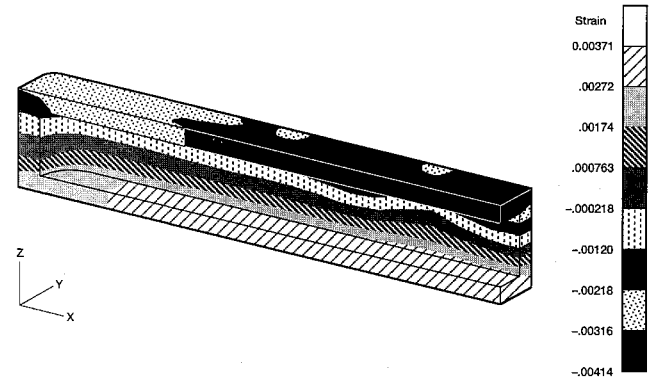

Fig. 12 *Z* strain in channel wall; elastic analysis.

mum magnitudes of the strains occur in the X direction (approximately equal to 0.7%). Also seen in Fig. 10 is the X strain, which is tensile in the top layer of the channel and compressive in the bottom layer. The middle of the channel has almost zero X strain.

Elastic–Plastic Analysis

Since the maximum elastically calculated stresses exceed the 0.2% offset yield strength of OFHC copper at 593°C by a factor of 25, plastic strains are implied to be very high in the critical regions. Keeping this in mind, a large-displacement elastic and perfectly plastic finite element analysis of the segment was performed. As in the case of the elastic analysis, the large-displacement elastic–plastic analysis is also based on an updated Lagrangian formulation. Some important results from elastic–plastic analysis are presented here.

The X-stress distribution in the channel obtained from an elastic–plastic analysis is shown in Fig. 13. The maximum X stress of 46.4 MPa contrasts with 766 MPa obtained from an elastic analysis. The Y- and Z-stress distributions in the channel are shown in Figs. 14 and 15, respectively. The maximum Y- and Z-stress magnitudes calculated from an elastic–plastic analysis were 34.2 and 14.9 MPa, respectively. The stress values obtained from an elastic–plastic analysis are significantly more realistic than those obtained from the elastic analysis.

The total X-, Y-, and Z-strain distributions in the channel are shown in Figs. 16–18. As expected, the X strain is tensile in the top layer and compressive in the bottom layer and has a maximum value along the x axis in the central region of the channel wall (Fig. 16). Similarly, because of Poisson's effect, the Z strain is compressive in the top layer and tensile in the bottom layer (Fig. 18). Figure 19 shows only the plastic component of the X strain in the channel. A comparison of this

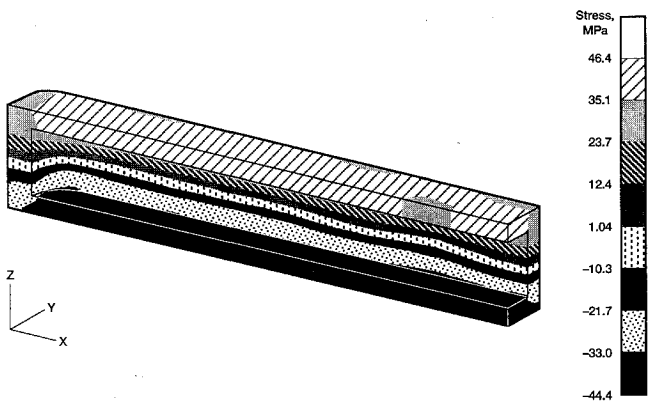

Fig. 13 X stress in channel wall; elastic–plastic analysis.

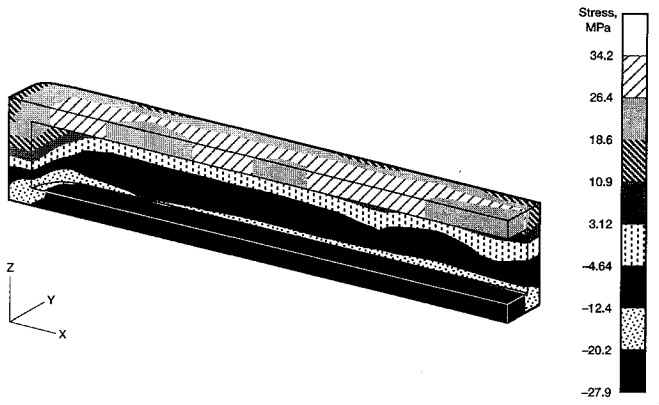

Fig. 14 Y stress in channel wall; elastic–plastic analysis.

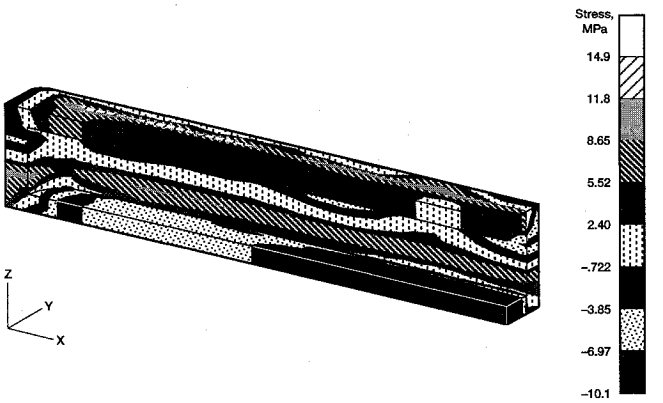

Fig. 15 Z stress in channel wall; elastic–plastic analysis.

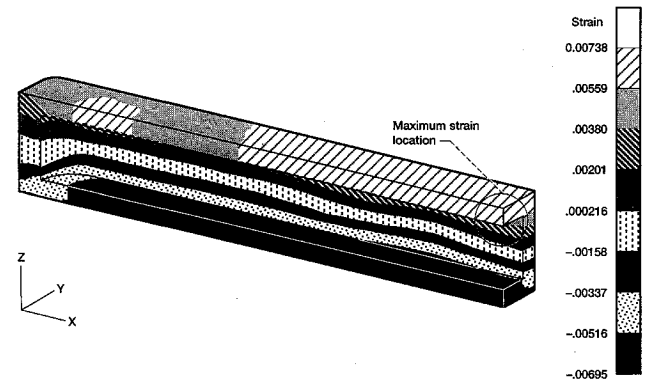

Fig. 16 Total X strain in channel wall; elastic–plastic analysis.

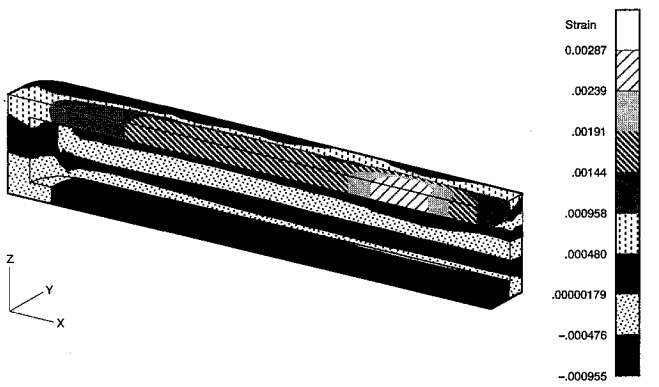

Fig. 17 Total Y strain in channel wall; elastic–plastic analysis.

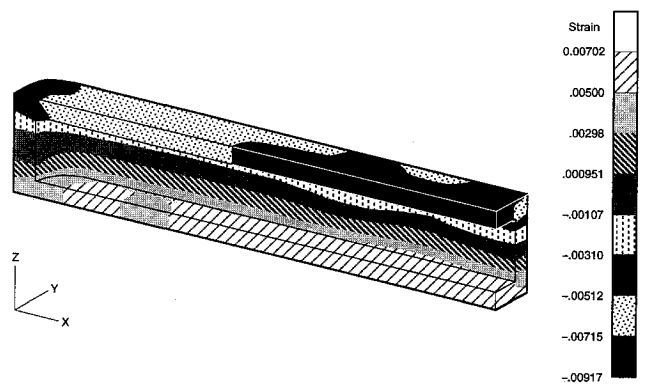

Fig. 18 Total Z strain in channel wall; elastic–plastic analysis.

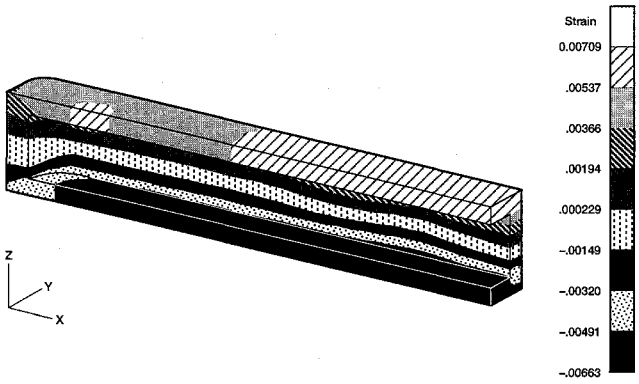

Fig. 19 Plastic X strain in channel wall; elastic–plastic analysis.

figure with Fig. 16 reveals that the deformation of the channel is largely plastic.

Life Analysis

The cyclic crack initiation life of the bend specimen was estimated by using the results from large elastic and large elastic–plastic structural analyses. Following the procedure of Manson and Halford[6] the maximum total effective strain range at the critical locations of the bend specimen were estimated by using the following expression:

Total effective strain ε_e

$$\varepsilon_e = (\sqrt{2}/3)[(\varepsilon_1 - \varepsilon_2)^2 + (\varepsilon_2 - \varepsilon_3)^2 + (\varepsilon_3 - \varepsilon_1)^2]^{1/2}$$

where ε_1, ε_2, and ε_3 are the principal strains.

The values of maximum total effective strain range for the bend specimen obtained from the elastic and elastic–plastic analyses are listed in Table 1.

Conway et al.[7] reported isothermal, strain-controlled, low-cycle fatigue test results for annealed OFHC copper at 538°C in a nonoxidizing argon atmosphere. These results are shown in Fig. 20 as total effective strain range vs cycles to crack initiation. An error band of $\pm \times 2$ is shown as dashed lines. The data were generated at a cyclic strain rate of 0.002 s^{-1}. Since this is within a factor of 2 (lower) of the rate of straining applied to the bend specimen, the fatigue curve is applicable to the assessment of its cyclic life. Outputs from the elastic and elastic–plastic analyses give the total maximum effective strain ranges at the critical locations of the specimen as 1.1 and 1.7%, respectively (see Table 1). From Fig. 20, these strain ranges are shown to correspond to cyclic lives of 500 and 190, respectively. Note that the maximum total effective strain ranges were determined from the results of elastic and elastic–plastic FEA performed at 593°C. Because no experimental data from OFHC copper are available at 593°C, the 538°C data were used to assess the cyclic life for the specimen. The justification for using the experimental data at 538°C to predict the cyclic lives from the results of analyses performed at 593°C lies in the fact that the tensile ductility of OFHC copper is insensitive to temperature. (Tensile tests of OFHC copper performed at NASA Lewis reveal a relatively small variation from 81 to 89% reduction of area over the temperature range from 20 to 593°C. Similar results have been reported for a zirconium–copper alloy.[9]) The low-cycle fatigue resistance is, therefore, also expected to be insensitive to temperature over the range of interest.[8]

The experimental life of the bend specimen was 109 cycles at 593°C. The elastic analysis predicts a longer cyclic life than that observed in experiments by more than a factor of 4. Although the elastic–plastic analysis also predicts a longer cyclic life for the bend specimen, the agreement between the prediction and experiment is much closer. Because the life predictions are based on a pure fatigue failure mode (exclusive of the bulged geometry), it is not surprising that the predictions exceeded the experimentally observed cyclic lives. In addition, the plates were tested in a life-reducing, oxidizing atmosphere, whereas the fatigue data were for an inert argon environment.

Table 1 Experimental and predicted cyclic lives of plate bend specimen

Analysis	Maximum total effective strain range at critical location, %	Life, cycles
Large elastic	1.1	500
Large elastic–plastic	1.7	190
Experiment	——	109

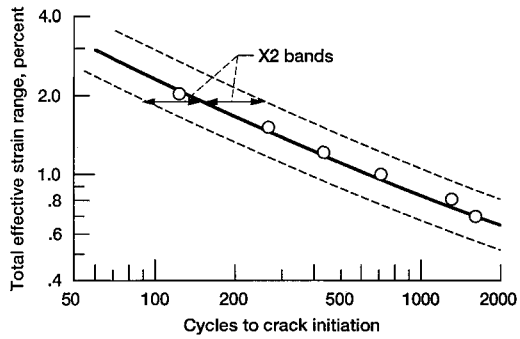

Fig. 20 Low-cycle fatigue resistance of OFHC copper at 538°C in argon at cyclic strain rate of 0.2% s^{-1} (Ref. 9).

Summary

Large-displacement elastic and elastic–plastic FEA were presented for a plate bend specimen with a single, centrally located, pressurized longitudinal cavity. The analyses incorporate an updated Lagrangian formulation. Using the results from these elastic and elastic–plastic FEA, the cyclic lives for crack initiation are assessed for the bend specimen. The elastic analysis predicted a longer cyclic life for the specimen than that observed in experiments by a factor of more than 4. The elastic–plastic analysis also predicted a longer cyclic life than that observed, but the prediction was in closer agreement with the experimentally determined cyclic life.

Appendix: Fabrication of Copper Plate Specimens

OFHC copper sheets (nominal 0.3 and 0.1 cm thick) were cut into 5 × 15 cm sections to match the 5-cm-wide channel die used for specimen fabrication. The thicker sheets were machined to produce a center chamber, 0.3 by 5 cm, with a thin gas transport passage (shown in Fig. 2). A 10-cm-long, 0.3-cm-diam stainless steel tube was inserted 5 cm into the gas transport passage to produce a gas pathway to the center chamber.

Prior to assembly operations, all surfaces of the copper sheets were mechanically cleaned with fine sandpaper to remove any copper oxide. Nickel–palladium (Ni-35.32Pd-9.63Cr-4.63Fe2.69B) brazing foil, 0.004 cm thick, was used for pressure brazing the two sheets together. This brazing alloy melts at a temperature between 945–996°C. Fifteen-cm-long sheets of the foil were cut and machined to produce a hole that matched the center chamber of the thick copper sheet. The brazing foil was secured to both surfaces of the thick copper sheet by a liquid brazing flux that acted as an adhesive. A debonding agent or Al_2O_3 wool was placed in the center chamber to prevent the flow of brazing material into the chamber. Thin copper sheets were placed on top of the brazing foil and secured with tape or copper rivets at the four corners. The

three-sheet assembly was covered with a release agent and placed into a vacuum hot press containing a 5-cm-wide channel die. The assembly was vacuum hot pressed (pressure brazed) by heating the die containing the sample to 982°C under a pressure of 3.4 MPa in a vacuum of 5×10^{-5} torr for a hold time of 1 h. The 0.2% offset yield strength of the OFHC copper at 593°C is 30 MPa.

References

[1]Quentmeyer, R. J., "Experimental Fatigue Life Investigation of Cylindrical Thrust Chambers," NASA TMX-73665, July 1977.

[2]Kazaroff, J. M., Jankovsky, R. J., and Pavli, A. J., "Hot Fire Test Results of Subscale Tubular Combustion Chambers," NASA TP-3222, Nov. 1992.

[3]Jankovsky, R. S., Arya, V. K., Kazaroff, J. M., and Halford, G. R., "Structurally-Compliant Rocket Engine Combustion Chamber—Experimental/Analytical Validation," NASA TP-3431, March 1994.

[4]Arya, V. K., and Arnold, S. M., "Viscoplastic Analysis of an Experimental Cylindrical Thrust Chamber Liner," *AIAA Journal*, Vol. 30, No. 3, 1992, pp. 781–789.

[5]"MARC General Purpose Finite Element Program," MARC Research Analysis Corp., Palo Alto, CA, 1992.

[6]Manson, S. S., and Halford, G. R., *Treatment of Multiaxial Creep-Fatigue by Strainrange Partitioning. Symp. Creep-Fatigue Interaction*, edited by R. M. Curran, American Society of Mechanical Engineers, New York, 1976, pp. 299–322.

[7]Conway, J. B., Stentz, R. H., and Berling, J. T., "High Temperature, Low-Cycle Fatigue of Copper-Base Alloys in Argon; Part I—Preliminary Results for 12 Alloys at 1000°F (538°C)," NASA CR-121259, Jan. 1973.

[8]Halford, G. R., Hirschberg, M. H., and Manson, S. S., "Temperature Effects on Strainrange Partitioning Approach for Creep-Fatigue Analysis," *Fatigue at Elevated Temperatures*, edited by A. E. Carden, A. J. McEvily, and C. H. Wells, American Society for Testing and Materials STP-520, 1973, pp. 658–667.

[9]Conway, J. B., Stentz, R. H., and Berling, J. T., "High Temperature, Low-Cycle Fatigue of Copper-Base Alloys in Argon; Part II—Zirconium-Copper at 482, 538, and 593°C," NASA CR-121260, Aug. 1973.